NAVAL POSTGRADUATE SCHOOL

MONTEREY, CALIFORNIA

THESIS

IMMORTAL SCIENCE OF DEAD WATER: EFFECTS OF INTERNAL WAVE DRAG ON SUBMERSIBLES

by

Marco Danieletto

September 2018

Thesis Advisor:	Timour Radko
Second Reader:	John E. Joseph

THIS PAGE INTENTIONALLY LEFT BLANK

REPORT DOCUMENTATION PAGE	*Form Approved OMB No. 0704-0188*

1. AGENCY USE ONLY *(Leave blank)*	**2. REPORT DATE** September 2018	**3. REPORT TYPE AND DATES COVERED** Master's thesis

4. TITLE AND SUBTITLE IMMORTAL SCIENCE OF DEAD WATER: EFFECTS OF INTERNAL WAVE DRAG ON SUBMERSIBLES	**5. FUNDING NUMBERS**
6. AUTHOR(S) Marco Danieletto	
7. PERFORMING ORGANIZATION NAME(S) AND ADDRESS(ES) Naval Postgraduate School Monterey, CA 93943-5000	**8. PERFORMING ORGANIZATION REPORT NUMBER**
9. SPONSORING / MONITORING AGENCY NAME(S) AND ADDRESS(ES) Naval Research Program, Monterey, CA 93941	**10. SPONSORING / MONITORING AGENCY REPORT NUMBER**

11. SUPPLEMENTARY NOTES The views expressed in this thesis are those of the author and do not reflect the official policy or position of the Department of Defense or the U.S. Government.

12a. DISTRIBUTION / AVAILABILITY STATEMENT Approved for public release. Distribution is unlimited.	**12b. DISTRIBUTION CODE** A

13. ABSTRACT (maximum 200 words)

Drag evaluation and prediction have always been integral to maximizing the efficiency of nautical vehicles. Yet, the total friction acting on a body moving in a fluid can be difficult to predict even today. In this regard, a still poorly understood source of drag with significant effects for vessels sailing in stratified waters is the so-called dead-water phenomenon. The dead-water phenomenon represents the dramatic increase in drag associated with radiation of internal waves created by the body itself. This phenomenon has been studied in the literature for surface vessels, but little attention has been given to the extent that dead-water affects submersibles. To address this issue, our research investigates the dead-water effects on a cylindrical body, comparing laboratory and numerical outcomes for both submerged and floating body experiments. Our results show more pronounced dead-water effects for submersibles than for boats, showing greater velocity loss (a factor of 1.28) and larger power loss (a factor of 2.4). These results have major implications for military operations. In particular, they show how a thorough understanding of dead-water effects can significantly increase the performance of naval vessels by improving their maneuverability and fuel consumption characteristics.

14. SUBJECT TERMS dead water, phenomenon, internal waves, stratified fluid, submerged body, floating body	**15. NUMBER OF PAGES** 63
	16. PRICE CODE

17. SECURITY CLASSIFICATION OF REPORT	**18. SECURITY CLASSIFICATION OF THIS PAGE**	**19. SECURITY CLASSIFICATION OF ABSTRACT**	**20. LIMITATION OF ABSTRACT**
Unclassified	Unclassified	Unclassified	UU

NSN 7540-01-280-5500 Standard Form 298 (Rev. 2-89) Prescribed by ANSI Std. 239-18

THIS PAGE INTENTIONALLY LEFT BLANK

Approved for public release. Distribution is unlimited.

IMMORTAL SCIENCE OF DEAD WATER: EFFECTS OF INTERNAL WAVE DRAG ON SUBMERSIBLES

Marco Danieletto
BS, University of Pisa, 2011
MS, University of Pisa, 2013

Submitted in partial fulfillment of the
requirements for the degree of

MASTER OF SCIENCE IN PHYSICAL OCEANOGRAPHY

from the

NAVAL POSTGRADUATE SCHOOL
September 2018

Approved by: Timour Radko
Advisor

John E. Joseph
Second Reader

Peter C. Chu
Chair, Department of Oceanography

THIS PAGE INTENTIONALLY LEFT BLANK

ABSTRACT

Drag evaluation and prediction have always been integral to maximizing the efficiency of nautical vehicles. Yet, the total friction acting on a body moving in a fluid can be difficult to predict even today. In this regard, a still poorly understood source of drag with significant effects for vessels sailing in stratified waters is the so-called dead-water phenomenon. The dead-water phenomenon represents the dramatic increase in drag associated with radiation of internal waves created by the body itself. This phenomenon has been studied in the literature for surface vessels, but little attention has been given to the extent that dead-water affects submersibles. To address this issue, our research investigates the dead-water effects on a cylindrical body, comparing laboratory and numerical outcomes for both submerged and floating body experiments. Our results show more pronounced dead-water effects for submersibles than for boats, showing greater velocity loss (a factor of 1.28) and larger power loss (a factor of 2.4). These results have major implications for military operations. In particular, they show how a thorough understanding of dead-water effects can significantly increase the performance of naval vessels by improving their maneuverability and fuel consumption characteristics.

THIS PAGE INTENTIONALLY LEFT BLANK

TABLE OF CONTENTS

THIS PAGE INTENTIONALLY LEFT BLANK

LIST OF FIGURES

LIST OF TABLES

THIS PAGE INTENTIONALLY LEFT BLANK

LIST OF ACRONYMS AND ABBREVIATIONS

C	Celsius
cm	centimeter
Fr	Froude number
Hz	Hertz
ITTC	International Towing Tank Conference
kHz	kilohertz
kg	kilogram
kW	kilowatt
kts	knots
m	meter
N	Newton
MITgcm	Massachusetts Institute of Technology General Circulation Model
psu	practical salinity unit
Re	Reynolds Number
s	second
S	salinity
T	temperature

THIS PAGE INTENTIONALLY LEFT BLANK

ACKNOWLEDGMENTS

This thesis is the result of many people's contributions and it represents the end of a journey that I could never have traveled alone.

First of all, I'm sincerely and deeply grateful to my thesis advisor, Professor Timour Radko. His expert advice and his passion for fluid dynamics guided me through the whole thesis process. The door of his office was always open, and he was always approachable; this journey would not have been so smooth and exciting without his patience and support.

I would also thank my second reader, Mr. John E. Joseph, for his availability, for his sincere interest on my project, for his precious advice, and for helping me in procuring all the equipment I needed for the laboratory experiment.

I cannot thank enough Dr. Justin Brown for his careful directions, endless patience, and continuous support. He dedicated countless hours for setting up my simulation and helping in the development of new code. I deeply appreciate all his meticulous comments that were enormously helpful for me, either to correct my English or to improve the scientific content of my thesis.

Special thanks also to Professor Timothy Stanton for guiding me among the several deceptions of conducting a lab experiment; his experience and his advice were crucial to get successful results. I also thank Mr. Keith Wyckoff for being such a supportive handyman—he always had the right solution to build optimally each component of my lab framework.

I thank the U.S. Navy for the valuable human and material resources that have been made available to me. In particular, I thank CDR Paula Travis for having been a great reference for these two whole years. She has been a serene guide who has always put me in a position to fully enjoy the best of this American experience. I thank also the IGPO staff members, who work every day to keep the NPS international community close, such a great environment where I made great lifetime friendships.

Furthermore, I thank the Italian Navy and all the people who, working in its behalf, have decided to trust me and further invest in my training by sending me here. I am aware of being privileged for this.

Finally, I would like to thank my classmates and my friends. Inter alia, my roommate, Petros, all the friends of the Italian community of Monterey and of the NPS international community. Last but not least, I would like to thank my family, who has been supporting me as if I had been close, even though I have been far away.

I. INTRODUCTION

A. BACKGROUND

Accurate predictions of drag are integral to maximizing the efficiency of vehicles in a number of transport sectors, including those pertaining to nautical and aeronautical systems. For instance, accurate drag predictions are needed by inertial positioning systems and consumption models, which are relevant to both surface and subsurface vessels. The nonlinear amplification of the drag can adversely affect the maneuverability and controllability of submersibles, which can elevate the risk of operational complications.

The drag on a body includes several components, such as the homogeneous form drag, viscous drag, and drag due to physical phenomena associated with specific environmental conditions, like in the case considered in this thesis. One of the major drag components is caused by the so-called dead-water phenomenon, a topic which so far has received little attention for submerged bodies. Dead-water represents the dramatic increase in the form drag associated with radiation of internal waves created by the body itself. The dead-water phenomenon usually occurs if the object is moving slowly enough to trigger intense wave-object interactions, which slows the body significantly.

For this effect to occur, the upper part of the ocean must be strongly stratified in density, due to either salt concentration or temperature. A parameter which is most effective in predicting whether stratification can affect a body moving in a fluid is the Froude number (*Fr*), which compares inertial and buoyancy forces:

$$Fr = \frac{v}{ND},$$

where v is the velocity, N is the Brunt-Väisälä frequency, and D is the diameter of the object. As demonstrated by V.W. Ekman [1], different values of the Froude number indicate whether the object is in the dead-water regime or not. Indeed, as pointed out by V. Duchene [2], the Froude number can be approximated as the ratio of the boat speed v to the maximum internal wave phase speed. When the Froude number is greater than

unity, radiated internal waves are slower than the submersible and do not significantly affect its motion. Conversely, when the Froude number is less than unity, the internal wave radiation becomes significant, which Ekman [1] noted leads to the dead-water phenomenon. Ekman also noticed how the dead-water regime can be inferred by the unsteady velocity patterns followed a towed object. He observed large oscillations compared to the mean value, and he related this amplitude to the towing force and the stratification. T. Miloh et al. [3] and O. V. Motygin et al. [4] further demonstrated that the drag associated with dead-water is maximal when the Froude number is slightly less than unity, i.e., the subcritical regime.

In the ocean, this phenomenon generally occurs in strongly stratified regions of the main pycnocline,[1] for instance, in the areas where glacier runoff flows into salt water without much mixing. Indeed, earlier observations of dead water were made north of Siberia, near the Nordenskiöld islands, by the Norwegian Arctic explorer Fridtjof Nansen [5], while sailing onboard the Fram on calm seas in 1893. In his diary, Nansen noted that he experienced a severe and inexplicable decrease of velocity, resulting in the loss of steering power. Nansen's observations inspired several studies of the dead-water phenomenon and are considered an essential source of information to the present day.

The first researcher to study and describe the physical features of the dead-water phenomenon in detail was [1]. In particular, Ekman performed laboratory experiments of this phenomenon with a two-layer tank setup. In addition to his aforementioned results, he observed much stronger drag in experiments with strong density stratification than in those with more homogeneous fluid. Relatively little consideration has been given to this problem for many years. Recently, however, more investigations of the topic have been published. In this context, much progress has been made with mathematical studies [3], [4], which have paved the way for new comparisons with laboratory work. M. J. Mercier et al. [6] performed such a comparison, focusing on the case of a semi-submersible object moving along the surface of fluids with two and three layers. Their conclusions revealed the robustness of the dead-water phenomenon, adding new explanations for the dynamics

[1] In a body of water, the pycnocline is the layer where the density gradient is greatest.

of the unsteady nature of the dead-water effect. Nevertheless, little attention has been given to studying the extent to which dead-water affects the drag for a fully submerged object as compared to one floating on the surface. This thesis aims to provide a deeper understanding of this particular case, specifically focusing on the possible impact that the dead-water phenomenon can have on naval operations in the real world.

B. NAVY RELEVANCE

Several regions of the world are characterized by a strong stratification in the upper ocean, and for many of these, the conditions are seasonal and easily predictable. For instance, in the Arctic, the fresh water coming from river runoff affects the upper ocean, resulting often in a favorable environment for the dead-water phenomenon. Furthermore, the Arctic Ocean is strategically crucial for the U.S. Navy for both military and economic reasons. The international context clearly presents the U.S. Navy with a number of good reasons to maintain its naval leadership in the area, ensuring presence and patrolling.

In terms of patrolling methods, submarines usually navigate at low speed (approximately 3 knots) to minimize noise and fuel consumption. Sea regions characterized by a strong pycnocline can easily have phase speeds up to 8 knots [7], [8], which implies that typical patrolling speeds can be subcritical and therefore susceptible to the dead-water phenomenon. Therefore, being able to estimate precisely how drag affects a submersible in dead water can improve the precision of inertial navigation systems, which nowadays still represent the primary positioning method for submarines. Another relevant application for the studied principle is the precise estimate of consumption for a submarine navigating at patrolling speed, ultimately resulting in greater consumption awareness and leading to energy savings, especially in the case of diesel propulsion.

In summary, a deeper understanding of the form drag that affects submarines during their patrolling activities in stratified waters is of significant benefit to the military in determining the degree to which the dead-water phenomenon impacts inertial navigation and energy loss. This study could improve the prediction of the consequent increase in fuel consumption and loss of maneuverability associated with dead water.

C. INTENT OF STUDY

The present work aspires to determine whether submerged bodies are affected by dead-water to the same extent as semi-submerged bodies. For this purpose, analogous laboratory and mathematical studies are performed and their results are compared. Both the submerged and semi-submerged experiments are performed in stratified and homogeneous fluids. The output data of this series of experiments is the body velocity, which is subsequently analyzed to infer how the dead-water drag behaves. At the same time, auxiliary mathematical simulations are performed using the Massachusetts Institute of Technology general circulation model (MITgcm) for conditions similar to those realized in the lab.

Prior to presenting the quantitative analysis of the dead-water phenomenon, it is important to note that the dynamics and typical values of the hydrodynamic drag in the submerged and semi-submerged cases are expected to be different. In the semi-submerged case, the energy loss due to the radiation of surface waves is substantial, while for the fully submerged objects, this effect is minimal. On the other hand, the circulation pattern around submerged bodies is more symmetric (see Figures 1 and 2), which may imply that the radiation of internal waves could be less effective than for surface vessels. Thus, the governing physics of the two different configurations are fundamentally dissimilar, as shown by the schematics in Figure 1 and Figure 2.

The material is organized as follows. Chapter II discusses the experimental setup and Chapter III presents the corresponding laboratory results. Chapter IV describes the MIT general circulation model (Marshall et al. [9]) setup and results. Afterwards, a comprehensive description and comparison of all components of this project are given in Chapter V. Finally, conclusions and suggestions for future work are presented in Chapter VI.

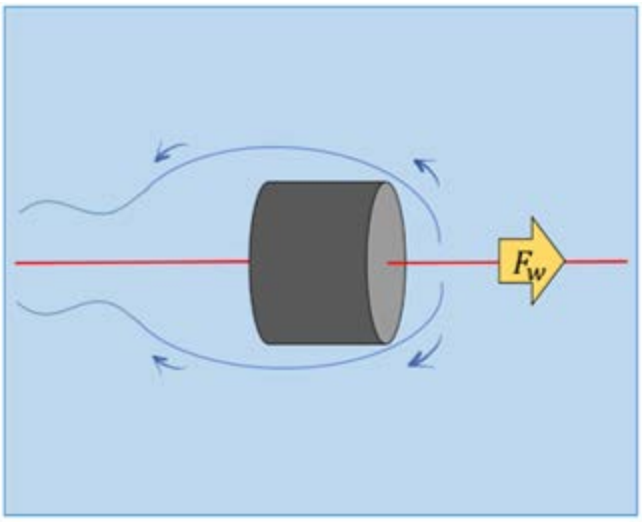

The cylindrical body in figure is attached to the red fishing line and towed by the weight force represented by the yellow arrow.

Figure 1. Submerged body fluid dynamics schematic

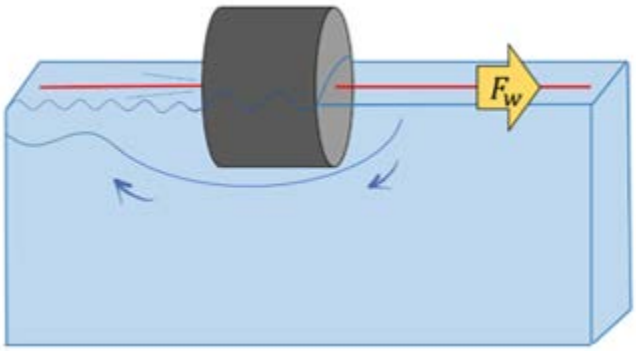

Figure 2. Semi-submerged body fluid dynamics schematic

THIS PAGE INTENTIONALLY LEFT BLANK

II. LAB EXPERIMENT SETUP

A. STRATIFICATION

Two environmental configurations are considered in this study: one with homogeneous fluid and one with stratified fluid. For the first case, the tank was filled with fresh tap water with a constant temperature of 20° Celsius. As a result, the density was also homogeneous with a value of $997\,\mathrm{kg/m^3}$. In the second case, the fluid was continuously stratified in temperature and salinity using the following procedures (Figure 3).

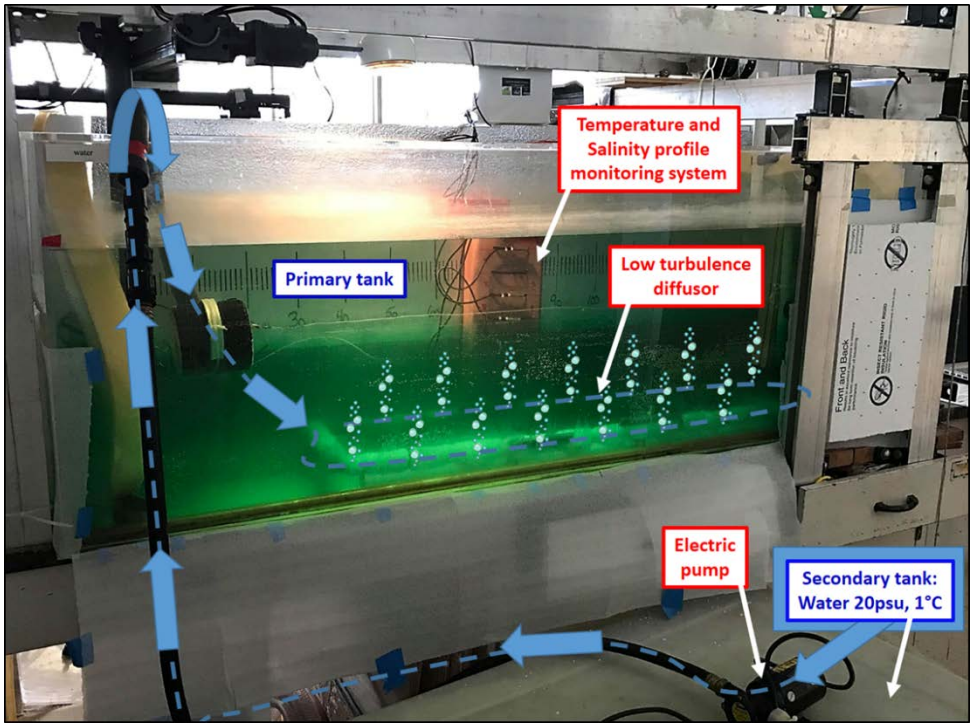

Figure 3. Laboratory tank setup

To create strong vertical stratification, an auxiliary tank is used in addition to the primary tank, and the water for the experiment was initially divided between the two tanks. While the water in the primary tank was fresh and at the environmental temperature of 20° Celsius, the water in the secondary tank was mixed with salt and ice

to increase its density up to $1{,}015\,\mathrm{kg/m^3}$. Afterwards, the water was pumped from the secondary tank into a thermally isolated pipe, entering the primary tank via a low turbulence diffusor situated at the bottom. When the water transfer was completed, the temperature and salinity profiles in the tank were measured with an RBR Concerto sensor. The RBR Concerto measures depth, temperature, salinity, and density anomaly with a sample frequency of 32 Hertz (Hz). In this sensor, depth is measured by a 200 kilohertz (kHz) acoustic altimeter. The altimeter was calibrated linearly to the surface of the fluid and the tank bottom. In addition, real-time temperature and salinity sensors were used to monitor any significant profile change during the experiments.

Experiments in stratified fluid with different configurations took place at different times, and therefore the resulting temperature-salinity (T-S) profiles were slightly dissimilar between the submerged and semi-submerged cases. For this reason, when results are introduced for each one of the stratified cases, they are always accompanied by the corresponding density profiles.

B. TOWING SYSTEM

In the following experiments, the towing system includes a fishing line with constant tension, which is used to move a body by a fixed horizontal force. The downward motion of the weight attached to the fishing line causes the boat to move, and therefore the ultimate towing force is mg, where m is the mass of the weight and g is the gravitational acceleration.

The wake-generating body is a cylinder 12 cm in length and 13 cm in diameter, while the falling weights used are of different masses, depending on the desired mean velocity of the object. The system is built to minimize friction, and the weights required to get the desired velocities are of only a few grams. The experiment takes place in a tank that has been filled up to 45 cm; this tank is 60 cm wide and 180 cm long. The experimental constraints limit the effective object run length to 130 cm. The force generated by the weight is transferred to the object by a low-elasticity fishing line passing through multiple low-friction pulleys. Two different configurations for the line path and

pulley placement have been used for the submerged and semi-submerged cases, as illustrated in Figure 4 and Figure 5 respectively.

To ensure that the results are not contaminated by experimental artifacts, we have adopted the following specific procedures. When the body is at its starting position, it is blocked with a hook and it stays at rest for at least one minute between one run and the next to guarantee that the internal waves from the previous run dissipate. The short time interval is sufficient to re-establish a calm state of the fluid due to two foam pillows placed at the ends of the tank, which efficiently dampen the internal waves. When the tank conditions are suitable for a new run and the appropriate weight is put in, an operator uses a thin stick to unhook the block and let the body travel along its guideline. Only when the object stops at the end of its trail is the run considered completed. The key diagnostic variable for each run is the time-record of the velocity of the propagating object, which is measured by an incremental rotary encoder.

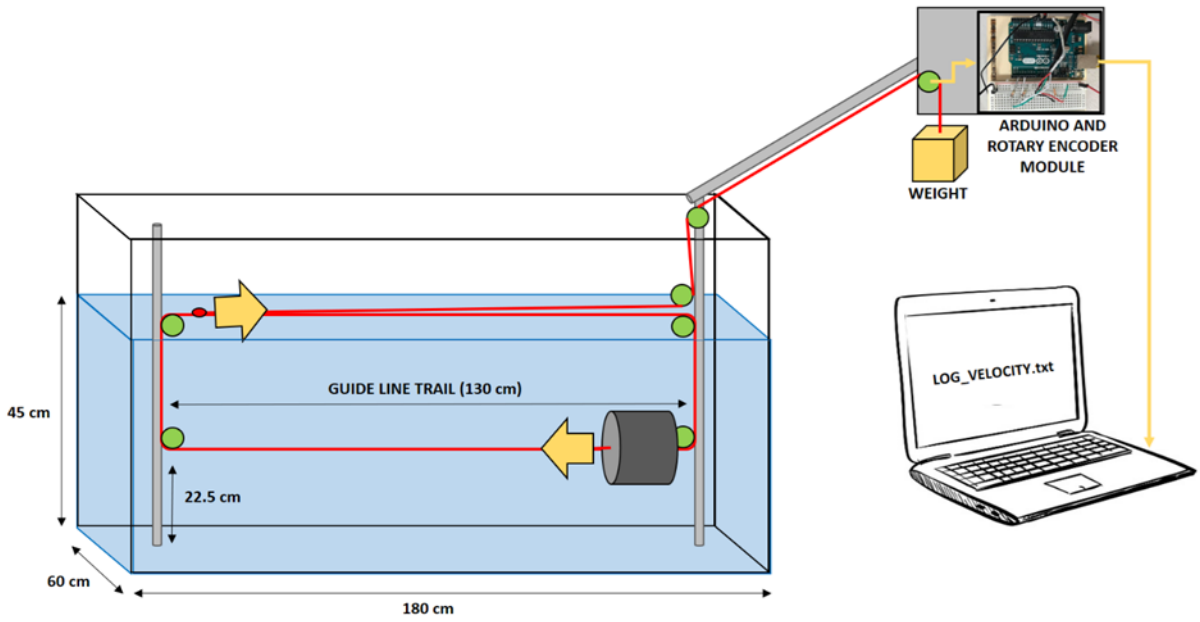

Figure 4. Schematic of lab configuration for submerged body case (not to scale)

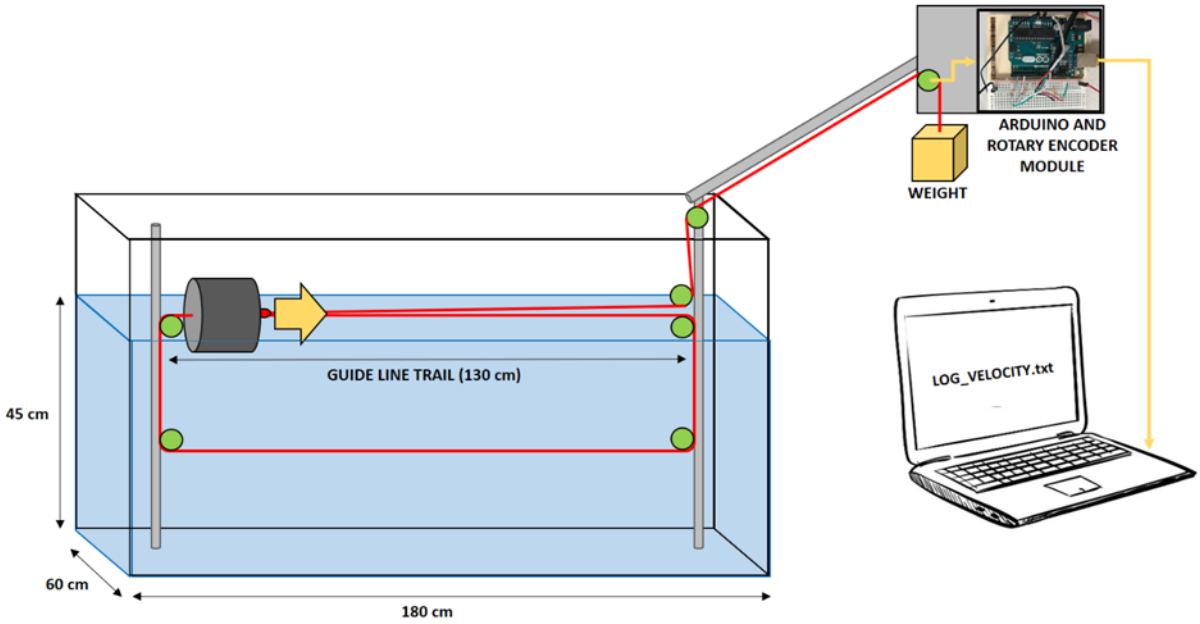

Figure 5. Schematic of lab configuration for semi-submerged body case (not to scale)

III. EXPERIMENTAL RESULTS

A total of 16 lab experiments have been performed during this project, the main characteristics of which are summarized in Table 1. For both the submersible and the float cases, four stratified runs were conducted with varying velocity. Two runs had speed less than, one greater than, and yet another one equal to the characteristic phase speed of internal waves in the tank. Additional runs in homogeneous fluid were performed using the same weight forces.

A. VELOCITY DIAGNOSTICS

In the lab experiments, the instantaneous velocity was measured with an incremental rotary encoder connected to an Arduino board. The velocity uncertainty of the instrument is 0.04 centimeters per second (cm/s). The measuring instrument setup adopted for this study is illustrated in Figure 6.

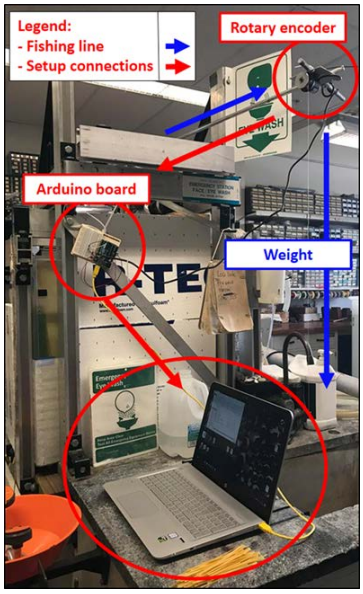

Figure 6. The setup for measuring the velocity pattern.

Table 1. The summary of laboratory experiments

Body	Fluid	*Run No.*	*T* [°C]	*S* [psu]	ρ [kg/m^3]	F_w [gr]	v_{av} [cm/s]	v_{ss} [cm/s]	$\frac{v_{ss}}{c}$	*Fr. No.*	*Re. No.*
SEMI-SUBMERGED	HOMOGENEOUS	1	19.5	0	997	27	14.61	18.16	N.A.	∞	17455
		2	19.5	0	997	30	18.16	26.88	N.A.	∞	21690
		3	19.5	0	997	34	23.12	31.69	N.A.	∞	27603
		4	19.5	0	997	38	27.14	37.61	N.A.	∞	32410
	STRATIFIED (phase speed 12.49 cm/s)	5	3–18	0–21	997–1015	27	6.41	8.73	0.70	0.36	5163
		6	3–18	0–21	997–1015	30	10.66	13.95	1.12	0.61	8584
		7	3–18	0–21	997–1015	34	15.85	21.68	1.74	0.91	12761
		8	3–18	0–21	997–1015	38	18.29	24.99	2.00	1.05	14721
SUBMERGED	HOMOGENEOUS	9	20	0	997	35	14.08	18.77	N.A.	∞	16818
		10	20	0	997	38	17.70	23.74	N.A.	∞	21137
		11	20	0	997	40	24.11	29.76	N.A.	∞	28789
		12	20	0	997	42	29.13	39.21	N.A.	∞	34790
	STRATIFIED (phase speed 12.76 cm/s)	13	3–18	0–20	997–1014	35	5.36	8.73	0.68	0.23	4313
		14	3–18	0–20	997–1014	38	9.77	13.95	1.09	0.42	7859
		15	3–18	0–20	997–1014	40	15.26	21.46	1.68	0.65	12275
		16	3–18	0–20	997–1014	42	19.24	24.99	1.96	0.82	15480

Shown for each lab experiment are the following parameters i from left to right: type of body, type of fluid stratification, identification number of the run, profile temperature range, profile salinity range, profile density range, weight mass, average velocity, steady-state velocity, steady-state velocity to phase speed ratio, Froude number, and Reynolds number.

The experiments eventually achieve a steady state where the driving force of a body equals the total drag force. In these experiments, this relation is expressed as follows:

$$F_w = D + F_{dyn}\ ,$$

where F_{w} is the towing weight force, D is the total drag force acting on the body, and F_{dyn} is the lab dynamic friction force. The mean velocity during the steady state is used to compare complementary experiments from the stratified and homogeneous cases. The difference in mean velocity between such cases is significantly larger for the stratified water case when the dead-water phenomenon is active.

Furthermore, as pointed out by Ekman [1] and Vasseur [6], the velocity of a body moving in active dead-water exhibits fluctuations of up to 85% of its mean value. These fluctuations raise the question of whether dead water can be interpreted as a steady state, although they do aid in identifying dead water. We characterize these velocity fluctuations using the standard deviation. Since in this experiment, the relative fluctuation is more relevant, standard deviation is presented both in canonical form as a measure of the effective velocity oscillation and in a form normalized to the mean velocity to properly make comparisons between different runs.

B. RESULTS

The results of the experiments listed in Table 1 are presented in the following sections, at first for the semi-submerged body and then for the submerged body. For each body configuration experiments in homogeneous fluid are compared with the ones in stratified fluid, in order to detect the experiments where the dead-water phenomenon is active.

1. Semi-Submerged Body

A total of eight experiments were performed using semi-submerged bodies. They are numbered from 1 to 8 with experiments 1 through 4 performed in homogeneous fluid and experiments 5 through 8 performed in stratified fluid. For both case studies, the experiments were ordered with increasing driving force weight. Note that the experiment pairs 1 and 5, 2 and 6, 3 and 7, and 4 and 8 were run with the same driving force, so in our analysis, they are referred to as complementary cases. The effects of dead water are expected in the stratified experiments where the Froude number is less than unity. Two

direct consequences of the dead-water phenomenon are detectable in the preliminary analyses conducted in this section. First, the comparison of the steady-state velocities between complementary experiments reveals faster motion for the homogeneous case, particularly when the body moving in the relative stratified case is in the dead-water regime. This consequently suggests greater drag acting on the object. Secondly, the normalized standard deviation reveals larger oscillations with the active dead-water regime.

Figure 7 shows the instantaneous velocity *v(t)* over time *t*, respectively, in cm/s and seconds. Analogous plots are presented for the other three case studies. All the experiments performed in homogeneous fluid showed small fluctuations, evidenced by the standard deviation measurements. In all experiments, as can be deduced from Figure 7, the body reaches a steady state after an initial acceleration phase. Note that, for faster cases, the steady-state interval is short due to the limited length of the tank, such as for experiment 4 (magenta).

The four experiments conducted in stratified fluid conclude the series of experiments carried out on the semi-submerged body. The stratification of the tank was created with vertically varying temperature and salinity. The density values varied from $997\,\mathrm{kg/m^3}$ on the surface up to $1015\,\mathrm{kg/m^3}$ on the bottom, as shown by the profile plotted in Figure 8A. The strong pycnocline results in high buoyancy frequencies (Figure 8B), creating ideal conditions for the dead-water phenomenon. Furthermore, the density gradient is approximately constant, resulting in the maximum phase speed of internal waves being nearly constant, given by [6]

$$c = \frac{Nh}{\pi},$$

where h is the characteristic length of the fastest internal wave mode. This length can be approximated as the depth of the tank, the largest relevant length scale of the system. Using the mean value of buoyancy frequency *N* from the lab, c is equal to 12.8 cm/s.

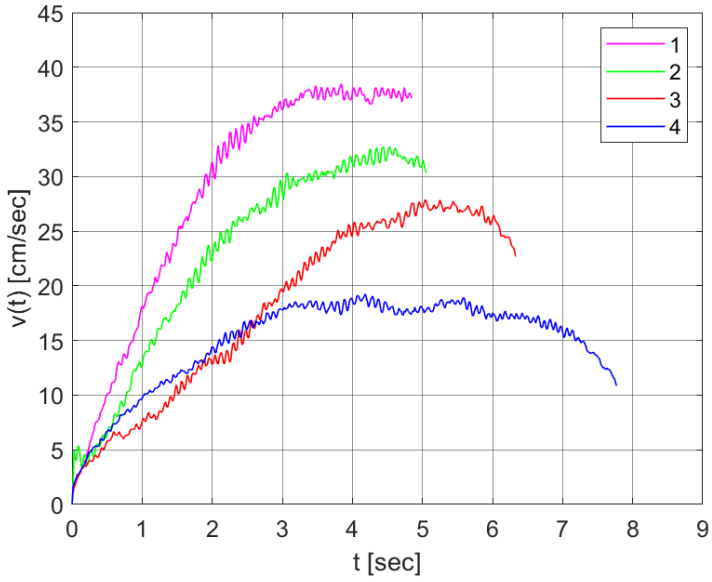

Figure 7. Velocity versus time for semi-submerged body in homogeneous fluid

Figure 9 plots velocity over time for the case in question; the maximum phase speed of the internal waves has also been plotted (dashed black line). When the instantaneous speed is less than the phase speed, the dead-water phenomenon is active. Additionally, in those circumstances, the velocity data show a greater presence of fluctuations. Experiment 5, for example, shows regular velocity fluctuations.

Key statistics for the semi-submerged body are summarized in Table 2. These data confirm the visual observations from the velocity plots in terms of estimated drag and fluctuations. Table 2 shows that, for a given stratification, greater towing weights lead to larger velocities, while for equal driving weight force, the body in stratified water moves slower than the one in homogeneous water. The latter is true especially in a comparison of the pair 1 and 5 (blue rows in Table 2), for which velocity is lower than the phase speed of the internal waves generated in the stratified fluid. This last observation suggests that there may be a larger dead-water drag force acting on the body in the slower stratified case.

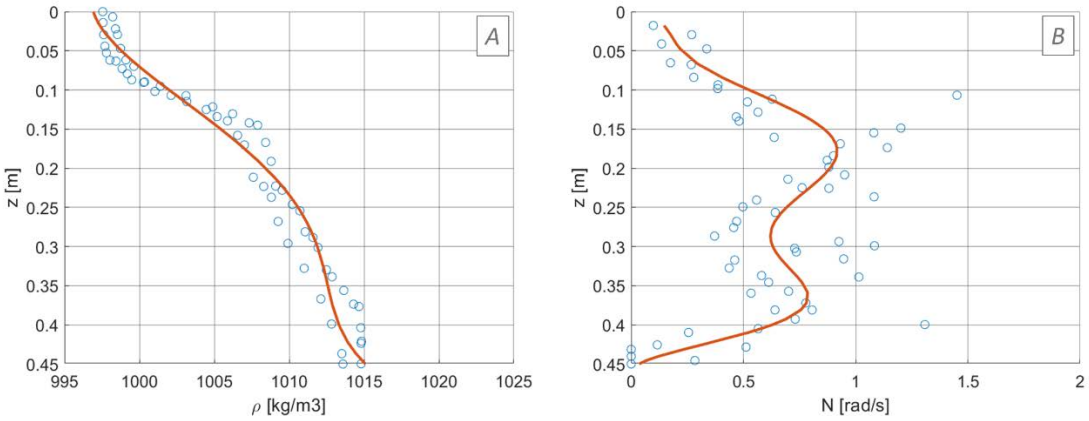

Figure 8. Lab tank density (A) and buoyancy frequency (B) profiles for semi-submerged body in stratified fluid

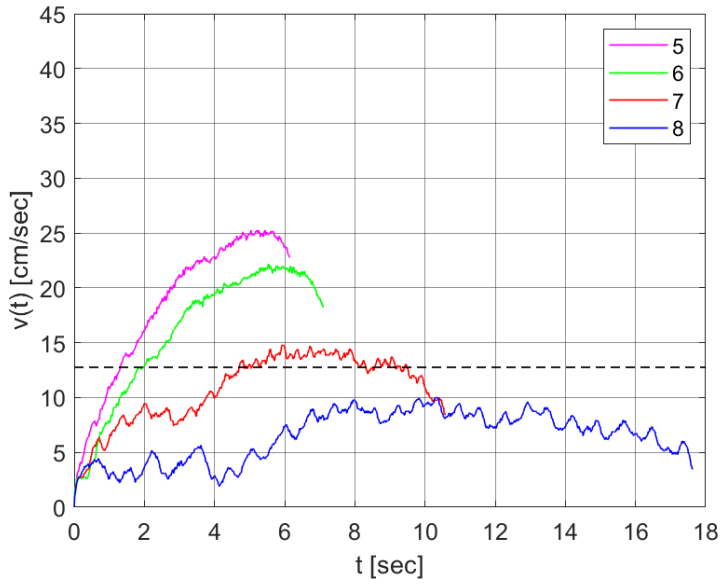

Figure 9. Velocity versus time for semi-submerged body in stratified fluid

In line with the visual observations, the standard deviation indicates that case 5 exhibits fluctuations to a larger extent than the other cases, suggesting the presence of dead water. Indeed, the normalized deviation of velocity for case 5 is larger than the one for case 8 by a factor of 10.63, which is significantly larger than for the semi-submerged body in homogeneous water for which this ratio is 2.74.

Table 2. Summary of results for semi-submerged body in homogeneous and stratified fluid

		No.	m_w [gr]	Fr	v_{ss} [cm/s]	σ_{vel} [cm/s]	σ_{vel}/v_{av}
SEMI-SUBMERGED BODY	HOMOGENEOUS FLUID	1	35	N.A.	18.16	0.4881	0.0269
		2	38	N.A.	26.88	0.6612	0.0246
		3	40	N.A.	31.69	0.5579	0.0176
		4	42	N.A.	37.61	0.3683	0.0098
	STRATIFIED FLUID	5	35	0.36	8.73	0.6404	0.0734
		6	38	0.61	13.95	0.3103	0.0222
		7	40	0.91	21.68	0.2468	0.0114
		8	42	1.05	24.99	0.1724	0.0069

2. Submerged Body

For the case of a submerged body, another eight experiments were performed, identified with numbers from 9 to 16. Numbering follows the same principle described for the semi-submerged body experiments. Complementary cases are 9 and 13, 10 and 14, 11 and 15, and 12 and 16. Diagnostic procedures used to estimate the mean velocity and fluctuations are the same, but this time the dead-water effects are more evident.

Figure 10 plots the submerged body time-series results in the same format as Figure 7. Similar to the semi-submerged body experiments, the submerged-body velocity in homogeneous fluid lacks the extreme fluctuations characteristic of dead water. The four experiments conducted on the submersible in stratified fluid conclude the lab work. The stratification is close to the one of the previous stratified case, with density values between $997\,\mathrm{kg/m^3}$ and $1014\,\mathrm{kg/m^3}$, as shown by the profile plotted in Figure 11A. Using the same calculation method previously used for *c* and the buoyancy frequency profile in Figure 11B, the maximum phase speed of internal waves is equal to 12.5 cm/s.

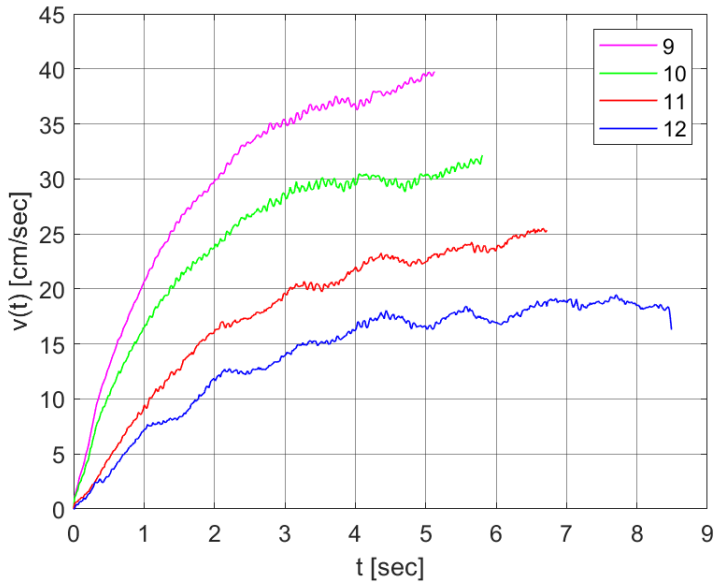

Figure 10. Velocity versus time for submerged body in homogeneous fluid

The time record of velocity for the submersible moving in stratified water is shown in Figure 12, where the maximum phase speed is represented by the dashed black line. Case 13 is clearly within the dead-water regime and shows characteristic fluctuations. Similar to the semi-submerged body, the body submerged in stratified fluid moves significantly slower than in the corresponding homogeneous case. The statistics of the submerged body motion are summarized in Table 3. The standard deviation confirms that case 13 shows the most substantial fluctuations attributable to dead water. Indeed, normalized deviation of velocity for case 13 is larger than the one for case 16 by a factor of 6.33, much larger than the corresponding pair for the submersible in homogeneous water, 1.93. This, combined with the observation of increased drag, confirms the presence of the dead-water phenomenon.

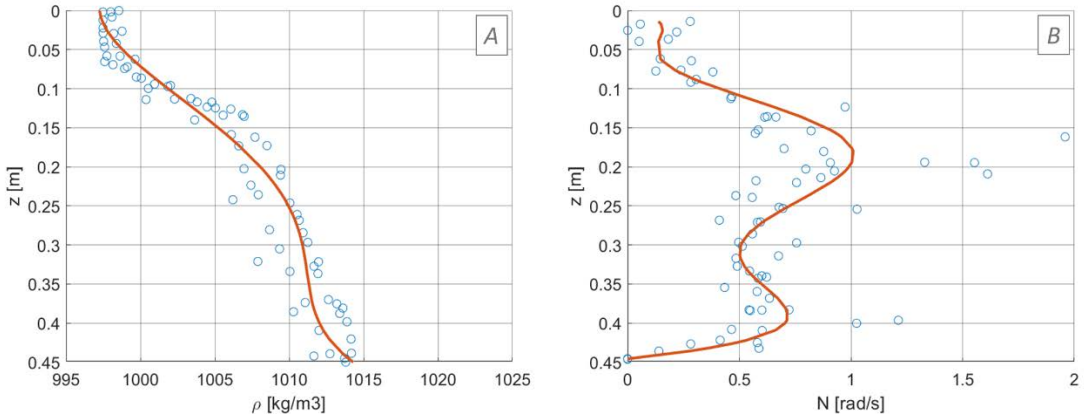

Figure 11. Lab tank density (A) and buoyancy frequency (B) profiles for submerged body in stratified fluid

Overall, the velocity fluctuations and the apparent drag anomalies have suggested the recurrent presence of dead water in a number of experiments. In more detail, cases 5 and 13 are the most affected by dead-water effects, respectively, for the semi-submerged and submerged bodies. Therefore, as this study aims at a deeper understanding of the dead-water phenomenon for submersibles, further attention is paid to case 13, which is reproduced numerically in the following chapter. These numerical experiments allow us to track and plot the fluid horizontal and vertical velocities, as well as the fluid's kinetic energy, all properties of the fluid that obviously would have been impossible to study in a lab experiment. Therefore, the ultimate goal of these mathematical simulations is to understand the differences between the fluid dynamics in homogeneous water and in the dead-water regime.

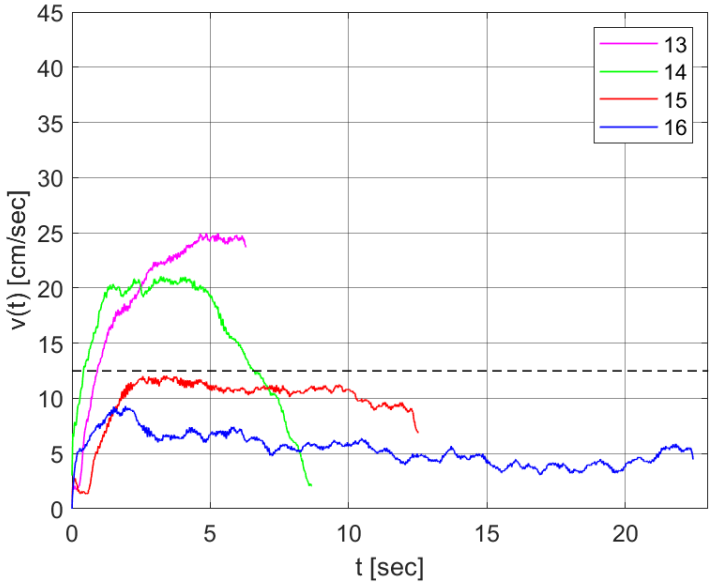

Figure 12. Velocity versus time for submerged body in stratified fluid

Table 3. Summary of results for submerged body in homogeneous and stratified fluid

		No.	m_w [gr]	Fr	v_{ss} [cm/s]	σ_{vel} [cm/s]	σ_{vel}/v_{av}
SUBMERGED BODY	HOMOGENEOUS FLUID	9	27	N.A.	18.77	0.2996	0.0160
		10	30	N.A.	23.74	0.2658	0.0112
		11	34	N.A.	29.76	0.4549	0.0153
		12	38	N.A	39.21	0.3262	0.0083
	STRATIFIED FLUID	13	27	0.23	8.73	0.4481	0.0513
		14	30	0.42	13.95	0.2021	0.0145
		15	34	0.65	21.46	0.8827	0.0411
		16	38	0.82	24.99	0.2026	0.0081

IV. NUMERICAL SETUP AND RESULTS

A. NUMERICAL SIMULATIONS

As mentioned previously, this study used the Massachusetts Institute of Technology General Circulation Model (MITgcm) to conduct numerical simulations. This finite-volume numerical model with non-hydrostatic capability was designed to perform simulations of the atmosphere and of ocean circulation. The model's governing equations are the incompressible Navier–Stokes equations, which result in a versatile model that can be used for the study of phenomena of many scales [9]. This flexibility of MITgcm allowed us to adapt it to our needs.

B. MODEL CONFIGURATION

Multiple model configurations were performed in MITgcm throughout this project. The model was designed to model the experiment carried out in the laboratory tank. Accordingly, the computational domain extended for 1,200 points in the *x*-direction, 400 in the *y*-direction, and 300 points in the *z*-direction, with a spatial resolution of 0.15 cm both vertically and horizontally, as shown in Figure 13. Impermeable, free-slip boundary conditions were imposed on the sides and bottom of the box to better simulate the environment of the tank.

In order to reproduce the features of lab experiment 13 (Table 1), the cylindrical body dimensions and position in the model corresponded directly to those of the laboratory counterpart. As illustrated in the schematic in Figure 13, the starting point of the body was at $\mathrm{x} = 15\mathrm{cm}$, $\mathrm{y} = 30\mathrm{cm}$, and $\mathrm{z} = 22.5\mathrm{cm}$. The body has a 13-cm diameter and a 12-cm length, and it was moved in the positive x-direction. The same tank density profile of the lab experiment was created using temperature gradient only, chosen to mimic the experimental density stratification from $997\,\mathrm{kg/m^3}$ at the top to $1015\,\mathrm{kg/m^3}$ at the bottom. The simulated diffusivity for temperature was $\kappa = 10^{-7}\,\mathrm{m^2/s}$, kinematic viscosity was $\mathrm{v} = 10^{-6}\,\mathrm{m^2/s}$, thermal expansion coefficient was $\alpha = 2 \cdot 10^{-4}\,\mathrm{kg/(m^3 \cdot °C)}$, and salinity contraction coefficient was $\beta = 7.4 \cdot 10^{-4}\,\mathrm{kg/(m^3 \cdot psu)}$.

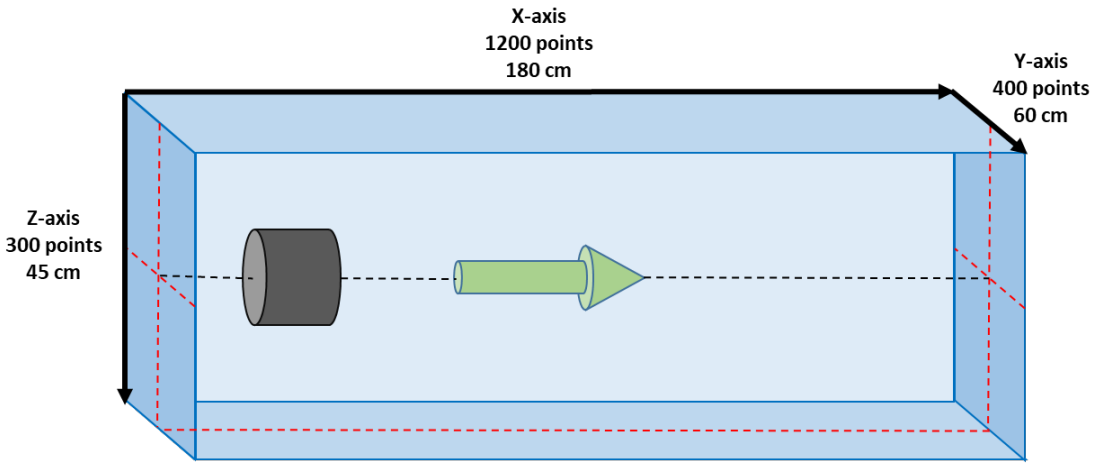

The body trajectory is plotted with black dashed lines, coordinates of the body's trajectory are plotted with dashed red lines.

Figure 13. Model configuration and dimensions (not to scale)

Taking as reference the 5 cm/s mean instantaneous velocity of lab experiment 13, two different simulations were performed. In these runs, the object started from rest and accelerated constantly with $a = 0.3\,\mathrm{cm/s^2}$, in homogeneous and stratified fluid. Having a constant acceleration allowed a gradual increase in the Froude number associated with the stratified case, consequently leading to observations of how pressure drag behaves with and without the dead-water regime. A summary of the main parameters of the two simulations carried out is available in Table 4.

C. RESULTS

The results for the two model runs are aimed at providing a deeper understanding of fluid dynamics in the comparison between lab experiments 9 and 13, which simulate a submerged body at subcritical speed respectively in homogeneous and stratified fluid. The comparison between these two cases reveals substantial differences, with features associated with internal waves evident in the stratified case.

Note that there are some differences in how lab and numerical experiments were planned, which have to be considered while analyzing the results. In fact, in the laboratory, speed fluctuations were observed during the steady state as a probable measure of dead-water activity index, while in the numerical simulation this cannot be

done because speed varies with constant acceleration. Indeed, in the lab experiments the constant parameter was the driving weight force, while in the computer simulations it was the acceleration of the object. Accordingly, the two numerical simulations were run with the same object displacement pattern in order to study the differences in the respective drag pressure force outcomes. Besides drag pressure force, the numerical experiments are compared also by fluid velocity patterns and kinetic energy.

Table 4. Numerical simulation overview

Fluid	**No.**	***v(t)* [cm/s]**	a **[cm/s^2]**	D_{av} **[N]**	***Fr***	***Re***
LINEARLY STRATIFIED (phase speed 12.5 cm/s)	1	0–9	0.3	0.0237	0 – 1.2	0–7976
HOMOGENEOUS	2	0–9	0.3	0.0183	N.A.	0–8056

For both cases, the *x*-component of the fluid velocity is plotted in Figure 14. In homogeneous water, the horizontal velocity is more turbulent, while in stratified water, more coherent structures are evident. In addition, the vertical velocity plots in Figure 15 show how the stratification leads to strong vertical motion immediately behind the body, which clearly results in internal wave formation. More precisely, two oppositely directed flows by generated internal waves are formed, and their intensity is stronger for the stratified case.

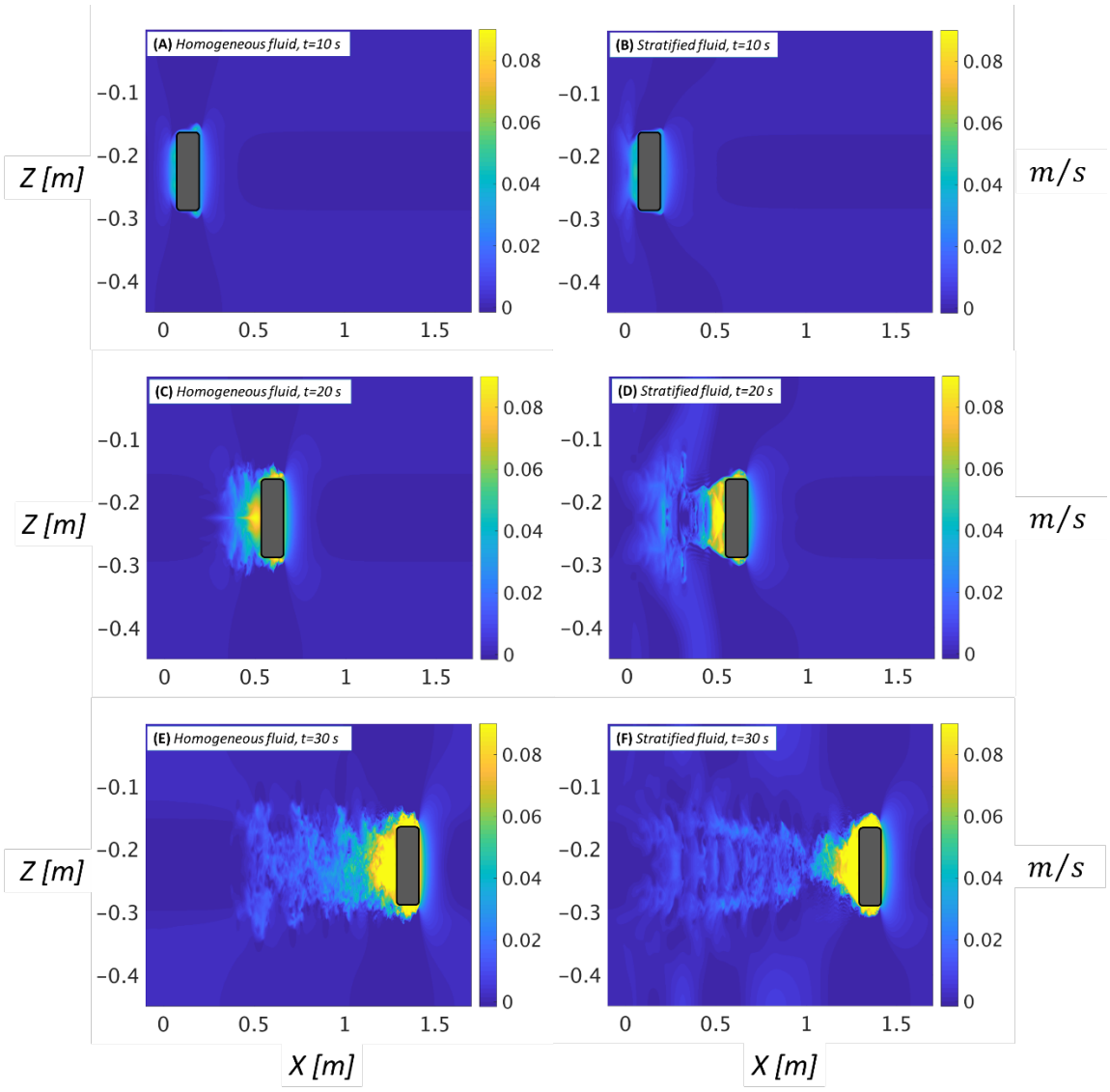

These plots represent the longitudinal vertical section of the tank on the central ordinate, which is the plane where the trajectory of the object lies. The sequence of plots depicts respectively the horizontal component of the fluid velocity at three equidistant moments, *t*=10s, *t*=20s, *t*=30s. The body in the simulation has a constant acceleration, so in those three time frames it has different instantaneous velocities, *v*=3cm/s, *v*=6cm/s, *v*=9cm/s, respectively.

Figure 14. Sequence of fluid horizontal velocity plots for homogeneous and stratified fluid, constant acceleration, $a = 0.3\ cm/s^2$

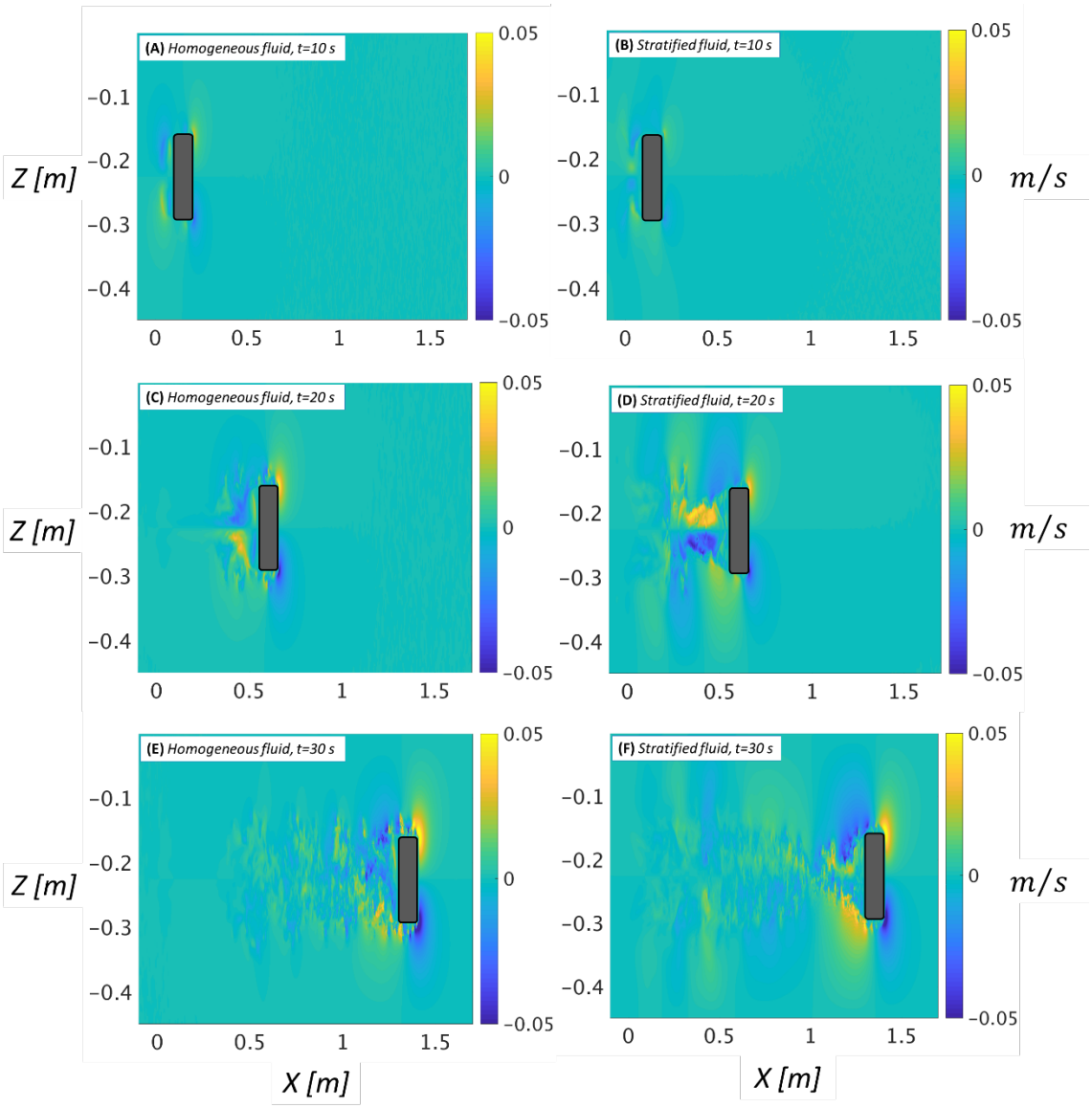

Figure 15. Sequence of fluid vertical velocity plots for homogeneous and stratified fluid, constant acceleration, $a = 0.3\ cm/s^2$

The central part of the bodies' wakes has similar features but opposite signs in the homogeneous and stratified cases, which can be seen in Figure 15C and Figure 15D, respectively. For a better understanding of the dynamics in this instant, the cross-sections of the two wakes have been plotted in Figure 16A and Figure 16B. The comparison between these two plots shows a different behavior of the stratified fluid, where the seemingly reversed directionality can be explained by internal waves.

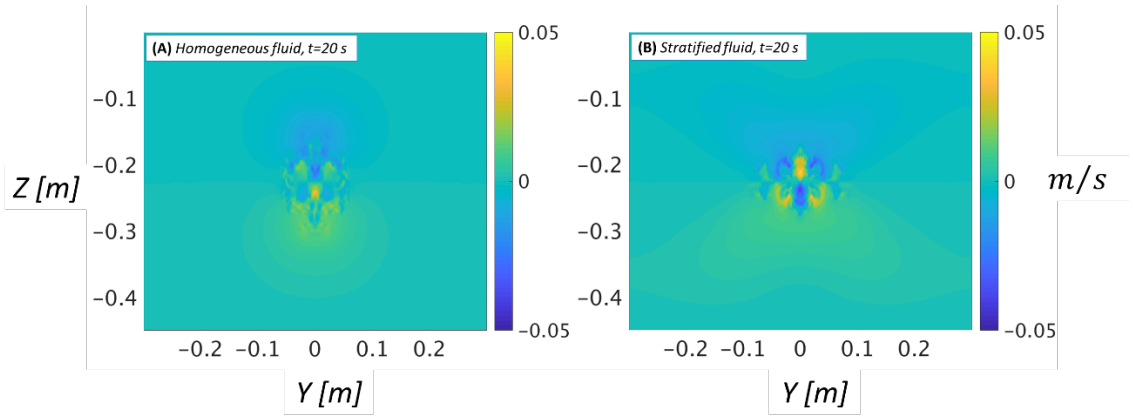

Figure 16. Wake cross-section of vertical velocity for homogeneous and stratified fluid, $t = 20\ s$, $a = 0.3\ cm/s^2$

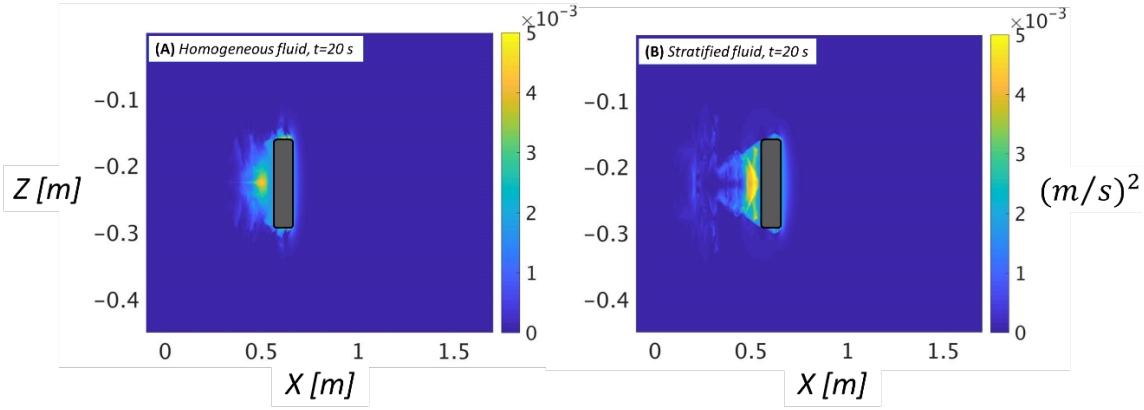

Figure 17. Comparison of fluid kinetic energy between homogeneous and stratified fluid, $t = 20\ s$, $a = 0.3\ cm/s^2$

The fluid kinetic energy is plotted in Figure 17. The kinetic energy in the wake can be considered as a measure of the energy loss that would be associated with the drag on the body. Indeed, from a visual comparison of the two plots, it is clear how in the stratified case the fluid throughout the whole tank is characterized by higher kinetic energy, suggesting larger energy dissipation. As an active dead-water regime is expected for the stratified fluid numerical simulation, this observation is consistent with greater drag acting on the body.

Finally, the more relevant outcome from the numerical simulation is the pressure drag force, which is plotted against the Froude number in Figure 18, where the Froude number increases linearly with velocity. As illustrated, for this numerical simulation the total drag is greater in stratified water when the Froude number is less than unity, which reaffirms Ekman's dead-water regime condition [1]: $Fr < 1$.

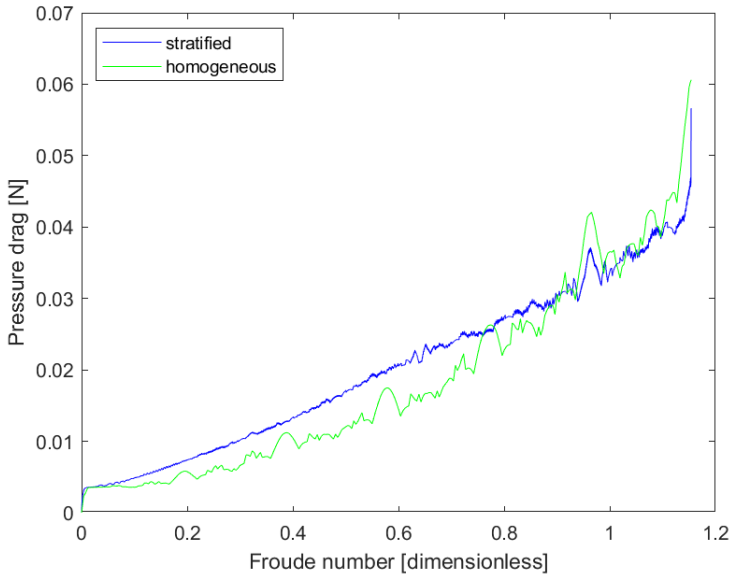

As known, the Froude number is impossible to calculate for the homogeneous case. However, the x-axis contains the Froude number related to the stratified case in order to show how the two data behave within and without the dead-water regime ($Fr < 1$).

Figure 18. Comparison of pressure drag versus Froude number for stratified and homogeneous fluid, $a = 0.3\ cm/s^2$

THIS PAGE INTENTIONALLY LEFT BLANK

V. ANALYSIS

A. LABORATORY EXPERIMENTS

The major finding of this study is that the dead-water phenomenon affects submersibles to a greater degree than surface vessels. The analysis for the lab results was conducted by comparing experiments with the same driving weight force in order to evaluate the extent of the dead-water effects case by case. Subsequently, we compared the overall results for the submersible and the surface vessel. The first diagnostic for the comprehensive final analysis is the ratio of the homogeneous velocity to stratified velocity evaluated for the same towing force, which will be referred to as the dead-water ratio and denoted by δ. Additionally, the total resistance was calculated and plotted for every lab experiment. Finally, the dead-water coefficient was calculated for both the lab and the numerical experiments, showing the relative weight of dead-water effects on total drag in each experimented case. In conclusion, final results of this thesis agree with the first dead-water observations done by Nansen.

1. Dead-Water Ratio

Our study introduced the so-called dead-water ratio, which is a measure of how velocity changes between lab experiments run with the same driving weight force in homogeneous and stratified water. It is therefore defined as:

$$\delta = \frac{v_s}{v_h},$$

which is expected to always be less than unity.

Values of the delta ratio for various velocities are plotted in Figure 19 for the submersible (blue) and the boat cases (green), respectively. Note that, for the submersible case, the ratio is generally lower, showing greater velocity variations for submersibles in stratified fluid than in homogeneous fluid. This effect is more pronounced when the body motion is slower than the phase speed, represented in the plot by the vertical dashed lines.

However, it is interesting to note that even for speeds well above the phase speed the delta ratio remains abundantly below the unit, touching a relative maximum of 0.7. This feature could be due to the fact that in the presence of a linearly stratified profile there is energy loss due to the formation of internal waves

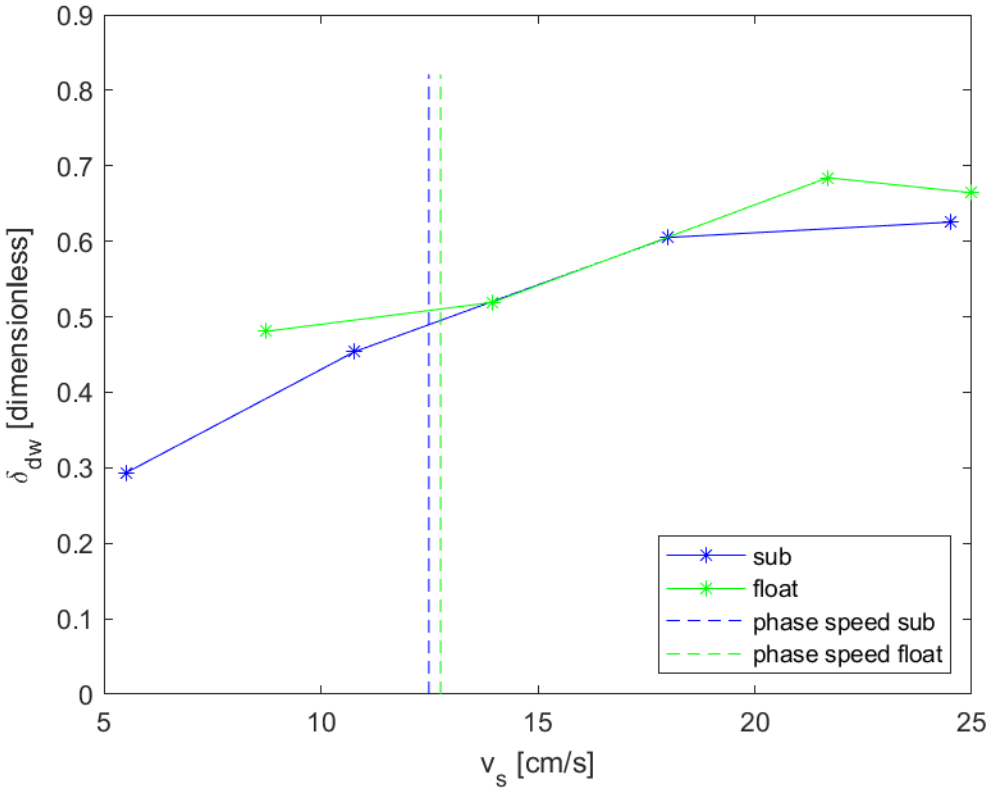

Figure 19. Mean stratified velocity versus delta ratio

2. Dead-Water Drag Coefficient

The primary indication of dead water is an increase in drag in stratified environments. This can be quantified using a dead-water drag coefficient, which characterizes the dead-water drag force in the same format as other types of drag. We thus define the total drag force as the following:

$$D = \frac{1}{2}\rho v^2 S\left(C_{dw} + C_p + C_f\right),$$

where D is the drag force, ρ is the water density, v is the body's velocity, S is the body's wetted surface area, and C_{dw}, C_{p}, and C_{f} are the dimensionless coefficients of dead-water drag, form drag, and viscous drag, respectively. The form drag coefficient of the cylindrical body is taken to be 1.15 for a Reynolds number in the range typical of our experiments ($10^3 - 10^5$); see Figure 12 from Chapter 3 of S. Hoerner [10], shown here in Figure 20. Finally, the viscous drag coefficient can be calculated using the ITTC-57 Model-Ship correlation line method. This method was established by the International Towing Tank Conference and is commonly used for naval engineering applications. The latter presents an expression for the viscous drag coefficient as follows:

$$C_{\mathrm{f}} = \frac{0.0075}{(\log_{10} Re - 2)^2},$$

where Re is the Reynolds number. For all the cases of these experiments, C_{f} was approximately 10^{-2}, which is much smaller than form drag and so is neglected.

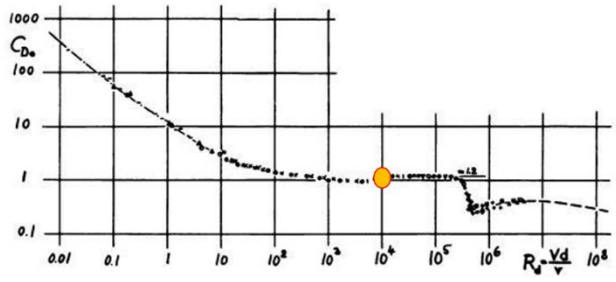

Figure 20. Cylinder drag coefficients as a function of Reynolds number. Source: [10].

Given two experiments of identical towing force but different stratifications, C_{dw} can be derived. The dynamic friction force associated with the pulley rig system can be represented as $F_{\mathrm{dyn}} = \mu_{\mathrm{dyn}} F_{\perp}$, where μ_{dyn} is the dynamic friction coefficient of the system and $F_{\perp}$ is the component of the force acting on the body that actively causes friction. Note that the dynamic friction force is independent of speed (and obviously of fluid stratification). Therefore, given the same towing weight for the homogenous and

stratified cases, respectively $F_{w,h}$ and $F_{w,s}$, once the system has achieved a steady state, we can write:

$$F_{w,h} = F_{w,s},$$

which, according to what was stated in Chapter III, Section A, is equal to:

$$D_h + F_{dyn} = D_s + F_{dyn}.$$

We assume that both dynamic frictional force components F_{dyn} match exactly; so, we have:

$$\frac{1}{2}\rho_h v_h^2 S C_p = \frac{1}{2}\rho_s v_s^2 S\left(C_p + C_{dw}\right),$$

where $\rho_{\mathrm{h}}, v_{\mathrm{h}}^2$ and $\rho_{\mathrm{s}}, v_{\mathrm{s}}^2$ are density and velocity for the homogeneous and stratified cases, respectively. Finally, C_{dw} is given by

$$C_{dw} = \frac{\rho_h}{\rho_s}\frac{v_h^2}{v_s^2}C_p - C_p.$$

In conclusion, given two experiments of identical towing force, C_{dw} can be easily calculated, and it depends exclusively on the drag coefficient, the density ratio, and the ratio of the steady-state velocities. Practically, the value of C_{dw} shows to what extent the dead-water phenomenon weighs on the total drag.

Following the illustrated method, C_{dw} was calculated and plotted for the laboratory experiments, as illustrated in Figure 21 for the semi-submerged case and in Figure 22 for the submerged case. In Figure 22 values of C_{dw} from the lab experiment are of the same order of magnitude and significantly higher for the submersible when in the dead-water regime; indeed C_{dw} for case 13 results in more than two times C_{dw} for case 5. At the same time, there is a substantial discrepancy between the values of C_{dw} for the submersible in the lab and those in the mathematical simulation (Figure 23). This may depend on alterations due to the lab framework drag, or perhaps the numerical experiment may not be able to reproduce dead-water effects exactly because the velocity oscillations may be a cardinal physical feature.

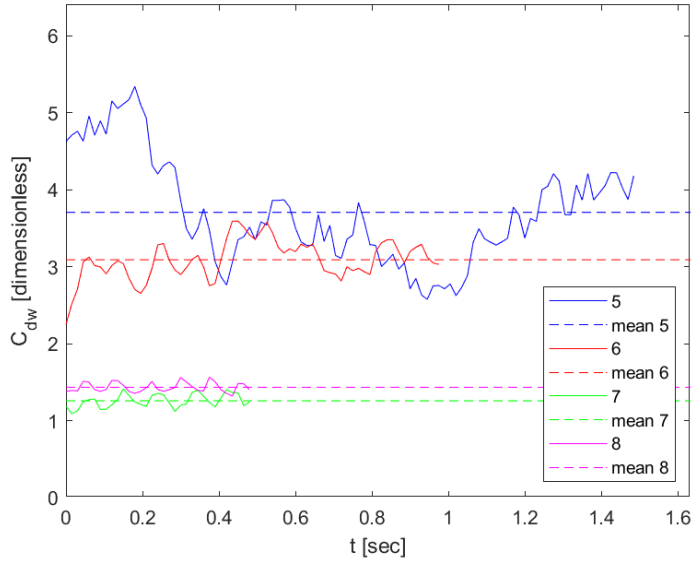

Figure 21. Time versus dead-water coefficient for near-steady-state sections of the lab experiments on semi-submerged body

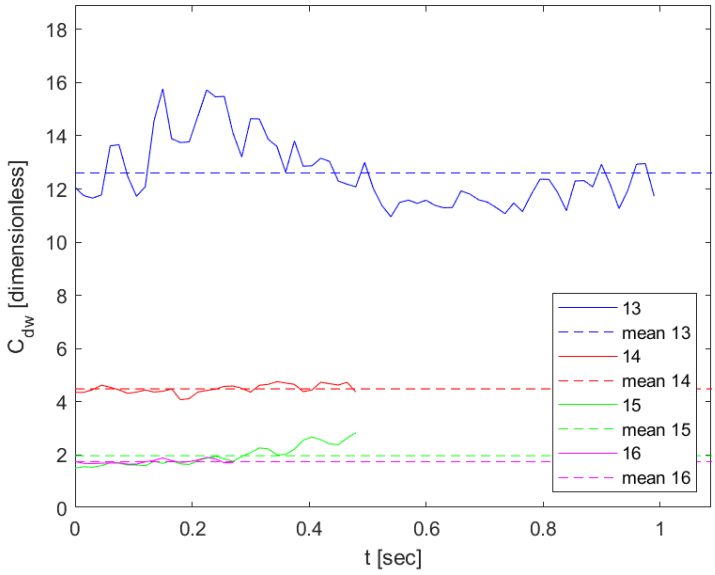

Figure 22. Time versus dead-water coefficient for near-steady-state sections of the lab experiments on submerged body

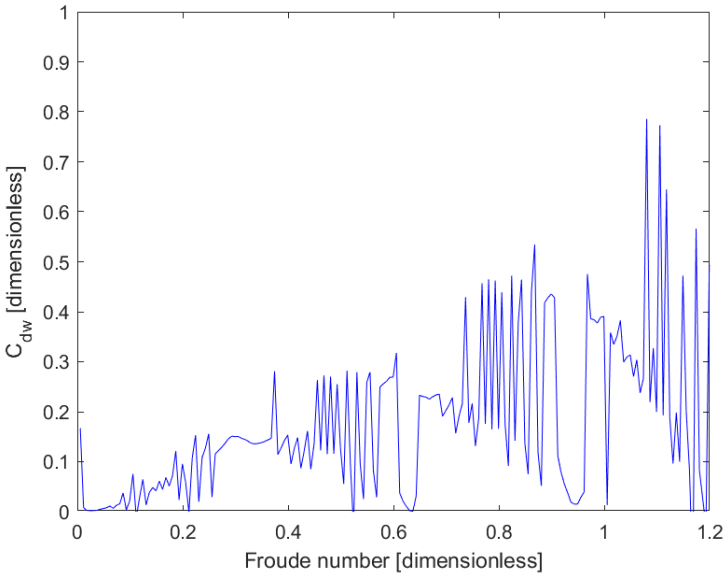

Figure 23. Froude number versus dead-water coefficient for the numerical simulation experiment for submerged body

3. Resistance

Resistance in grams is a measure of the real resistance experienced in the lab experiment by the cylindrical body. It is calculated as the ratio of drag force in Newtons to the gravitational acceleration, in grams:

$$R = \frac{D}{g},$$

where D is in Newtons. This quantity was also plotted by Ekman [1] and then recently used by Vasseur [6].

In Figure 24, the resistance is plotted for different steady-state mean velocities, for both the submersible and boat cases. In general, the body experiences stronger drag when it is submerged. In the subcritical region, where velocity is slower than phase speed, lower velocities result in higher resistances experienced by the submerged body. For the boat case, conversely, resistance has a relative maximum close to the phase speed value, consistent with what was previously shown by Ekman and Vasseur. For velocities higher than the phase speed, resistance increases with velocity as is physically

reasonable. In conclusion, this shows that resistance for submerged and semi-submerged objects have different behaviors, suggesting that drag of submersibles may be significantly affected by dead water and when traveling with velocities substantially lower than the fastest internal wave phase speed. The resistance for even lower velocities would make for reasonable future investigation but was impossible to explore in this work due to the static friction of the lab framework.

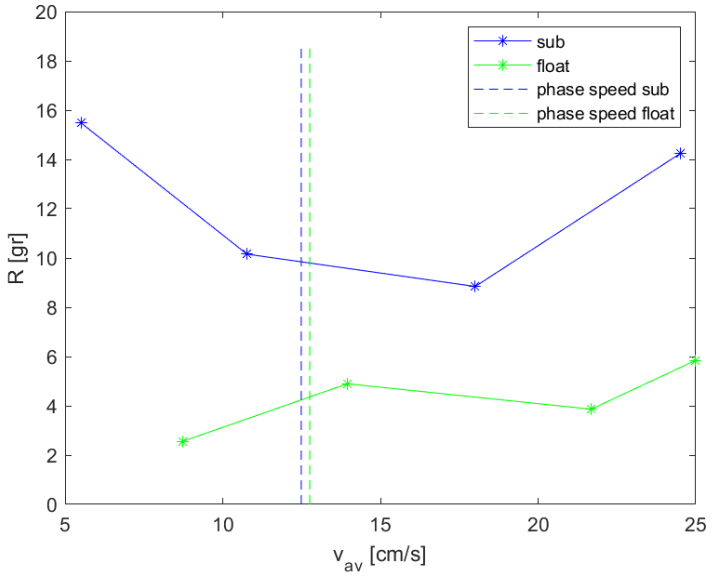

Figure 24. Mean velocity versus resistance in grams

B. THE ANALYSIS OF NANSEN'S OBSERVATIONS

In light of this study, we intend to quantify the operational effects of the phenomenon under analysis, focusing on Nansen's original observations. As written by Nansen in [5], his ship experienced large dead-water resistance. According to Nansen's narration, the Fram's maximum speed was 4.5 knots (kts) in ideal conditions, given maximum power delivery by its 164-kW triple-expansion steam engine, which supposing an arbitrary engine efficiency of 25% we can consider effectively equal to 41 kW. Nevertheless, anomalously, Nansen reported that while navigating in strongly stratified water, the speed at full ahead was reduced to 1.25 ± 0.25 knots.

The results of a numerical simulation recently published by J. Grue [11] have further addressed Nansen's experience. Grue claims that the dead-water coefficient acting on the Fram was equal to $C_{\mathrm{dw}} = 0.1$, considering only the viscous friction as an additional source of energy dissipation, calculated by Newman [12]: $C_{F_1} \cong 0.0022$ in normal conditions and $C_{F_2} \cong 0.0027$ in dead water.

There are two aspects, however, that were wrongly neglected by Grue. First, he did not consider the estimated maximum power of the Fram's engine, which we consider to be equal to 41 kW (estimating a 25% engine efficiency) [5], almost seven times greater than the value calculated by Grue's assumptions. Second, in Grue's calculations form drag is completely neglected, even if typical values of form drag are far larger than viscous drag. Ergo, neglecting viscous drag and equalizing P_1 to the estimated maximum rowed power $P_{max} = 41\ kW$, we derive the consequent value of form drag C_p:

$$P_1 = D_1 v_1 = \frac{1}{2}\rho v_1^3 S C_p = P_{max}\,,$$

$$C_{\mathrm{p}} = \frac{P_{max}}{\frac{1}{2}\rho v_1^3 S} = 0.0144\,,$$

where the wetted surface area is taken to be $S = 450m^2$ [5] and the estimated density, $\rho = 1020\,\mathrm{kg/m^3}$. The obtained estimate for C_{p} compared with form drag for a half-streamlined body ($C_{\mathrm{p}} = 0.09$, [13]) seems to be a reasonable value. At this point the balance $P_1(v = 4.5kts) = P_2(v = 1.25kts)$ is imposed to derive the correspondent value for C_{dw}:

$$\frac{1}{2}\rho v_1^3 S C_p = \frac{1}{2}\rho v_2^3 S(C_p + C_{dw})\,,$$

$$C_{dw} = \frac{v_1^3}{v_2^3} C_p - C_p = 0.6576\,,$$

which gives $C_{dw} = 0.6576$, a larger value than Grue's estimate of 0.1. Figure 25 illustrates how Grue's estimate remains lower than the calculated C_{dw} for all the reasonable engine efficiency values.

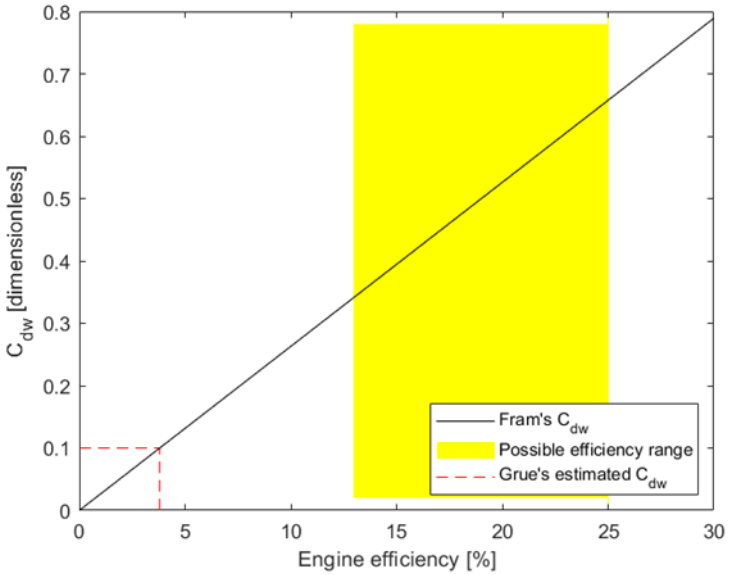

Figure 25. Fram's dead-water coefficient versus possible engine efficiencies

Moreover, this value for C_{dw} is closer to the range of values experienced by the semi-submersible body in our lab experiment ($C_{dw} \cong [4,16]$), considering that the density gradient simulated in the lab was probably much stronger than typical profiles found in the real world. In addition, the keeping in mind that the shape of our cylindrical body differed from that of the Fram's hull, we might consider that dead-water may affect the two bodies to different extents.

Note that these new parameters reveal a huge difference in power between ordinary conditions and the dead-water regime. Indeed, calculating the power consumed by the Fram to navigate at speed v_2 in a homogeneous fluid we get $P_1(v = 4.5kts) = 0.9\ kW$, while navigating at the same speed in a dead-water regime the consumed power would have been $P_2(v = 1.25kts) = 41\ kW$. Therefore, as clearly demonstrated, there is a huge difference that clearly shows the relevance of dead-water effects in the real world.

In conclusion, according to the relations previously demonstrated by the comparison between semi-submerged and submerged bodies, the large drag experienced by Nansen's Fram would have been even larger for a submarine with similar dimensions experiencing the same environmental conditions.

THIS PAGE INTENTIONALLY LEFT BLANK

VI. CONCLUSIONS

The major finding of this study is that the dead-water phenomenon does affect submersibles to a larger extent than surface vessels. This has been shown through the use of analogous lab and numerical experiments and by comparing the outcomes with the original field observations reported by Nansen during his Fram expedition.

A number of laboratory experiments have shown clear features associated with dead water, such as velocity fluctuations and very large differences in velocity for the same towing weight force. The lab analysis revealed dead-water ratios of the same order as in Nansen's observations, $\delta \cong (0.25, 0.5)$. Even more importantly, they revealed an overall larger dead-water ratio and drag coefficient for the submerged object than for the semi-submerged one, with amplification factors up to 1.5 and 3.3 respectively.

Furthermore, the dead-water experiments revealed larger drag for the stratified case even well above the dead-water regime ($\delta \approx 0.7$), probably due to energy loss for internal waves formation. If confirmed by field observation, this feature would be very significant especially for open water shipping vessels, which have typical arctic routes passing thru regions affected by rivers runoff, such as the waters between Kara Sea and Chukchi Sea, extended over 1,900 nautical miles. For a similar distance to lose 30% of velocity corresponds to a huge increase on fuel expenses, on the order of $100K.

The numerical experiments allowed us to analyze the properties of fluid that are inaccessible through laboratory work alone, achieving a deeper understanding of how the fluid acts in a dead-water regime. In this regard, clear differences have been noted between the body's wake moving in a homogeneous fluid and the one of a body moving in an active dead-water region. The latter shows dynamic features of the wake, clearly due to the buoyancy of the fluid, which leads to internal wave formation. Therefore, the mathematical simulations analysis revealed consistency with the dead-water phenomenon theory in terms of fluid behavior. Furthermore, the form drag pressure output is larger for the case in the active dead-water regime, which is what we physically expected.

Nonetheless, comparing the dead-water drag coefficient for the submerged body between the laboratory and numerical experiments, we find a substantial difference. This difference could be due to the inability of our numerical setup to simulate velocity fluctuations in the condition of a body towed by constant force, characteristics of the phenomenon that may be critical for an exact replica of its effects in the real world.

In order to place our laboratory-based conclusions in their historical context, we analyzed Nansen's early field observations of the dead-water phenomenon and compared them to our results. Nansen experienced a dead-water ratio of 0.27 and a drag coefficient of 0.66. While the delta ratio is in line with our lab experiments, the dead-water coefficient is definitely lower than the one observed in our lab, which for the cases in an active dead-water regime was between 4 and 16. This difference may depend on several factors. The most plausible explanation is the difference in shape between the object used in the lab and that of Fram's hull. This variance may have different wave-generating properties. Another reason could be associated with the inherent uncertainties of the extrapolation of lab-based results to very different oceanic scales. The strong gradient created in the laboratory experiment may have affected our cylindrical body to a larger extent than the Fram. Indeed, even though the density profile data from Nansen's observations are not available, we know that at the time he was navigating near Nordenskiöld islands, a region typically affected by river runoff. Therefore, according to what has been observed in similar areas, it is reasonable to expect that Nansen experienced a profile with density changes from 1015 kg/m^3 to 1025 kg/m^3 in the top 20 meters of the ocean. Conversely, in the lab density was changing from 997 kg/m^3 to 1015 kg/m^3 in a 45 cm deep tank.

In conclusion, the presented study shows that the results obtained in the laboratory are reasonable; therefore, it is expected that dead-water effects for submarines will be greater than that for surface vessels. These conclusions are of significant relevance for the U.S. Navy, particularly in regard to submarines patrolling in the Arctic Ocean. Indeed, it has been suggested by our measurements of the dead-water ratio that when the Arctic Ocean presents a strong stratification on its upper part a submarine can be slowed to up to one-fifth of its typical velocity in low-stratification regions for the

same engine power. Therefore, considering the potentially significant implications of the dead-water phenomenon, it may be prudent to avoid the dead-water regime by traveling below the pycnocline. In addition, this study can lead to greater accuracy in fuel consumption estimates and maneuverability awareness.

THIS PAGE INTENTIONALLY LEFT BLANK

LIST OF REFERENCES

[1] V. W. Ekman, “On dead water.” in *The Norwegian North Polar Expedition 1893–1896: Scientific Results,* vol. 5, F. Nansen, Ed. Christiania, Norway: J. Dybwad,1906.

[2] V. Duchene, “Asymptotic models for the generation of internal waves by a moving ship, and the dead-water phenomenon,” *Nonlinearity,* no. 24, pp. 2281–2323, 2011.

[3] T. Miloh, M. P. Tulin, and G. Zilman, “Dead water effects of a ship moving in stratified seas,” *J. Offshore Mech. Arct. Eng.*, no. 115, pp. 105–110, 1993.

[4] O. V. Motygin and N. G. Kuznetsov, “The wave resistamce of a two dimensional body moving forward in a two-layer fluid,” *J. Eng. Math.*, no. 32, pp. 53–72, 1997.

[5] F. Nansen, *Furthest North: The Epic Adventure of a Visionary Explorer.* New York, NY, USA: Skyhorse Publishing, 1897.

[6] M. J. Mercier, R. Vasseur, and T. Dauxois, “Resurrecting dead water phenomenon,” *Nonlinear Processes Geophys.*, no. 18, pp. 193–208, 2011.

[7] L. D. Talley, G. L. Pickard, W. J. Emery, and J. H. Swift, *Descriptive Physical Oceanography*. London, England: Academic Press, 2011.

[8] A. E. Gill, *Atmosphere-Ocean Dynamics*. London, England: Academic Press, 1982.

[9] J. Marshall, C. Hill, L. Perelman, and A. Adcroft, “Hydrostatic, quasi-hydrostatic and nonhydrostatic ocean modeling,” *J. Geophys. Res.: Oceans Banner,* no. 102, pp. 5733–5752, 1997.

[10] S. Hoerner, *Fluid-dynamic Drag: Theoretical, Experimental and Statistical Information*. Bakersfield, CA, USA: Published by the author, 1965.

[11] J. Grue, “Nonlinear dead water resistance at subcritical speed,” *Physics of Fluids,* no. 27, 2015.

[12] J. N. Newman, *Marine Hydrodynamics*. Cambridge, MA: MIT Press, 1977.

[13] T. E. Faber, *Fluid Dynamics for Physicists*. Cambridge, UK: Cambridge University Press, 2010, pp. 264–268.

THIS PAGE INTENTIONALLY LEFT BLANK

INITIAL DISTRIBUTION LIST

1. Defense Technical Information Center
   Ft. Belvoir, Virginia

2. Dudley Knox Library
   Naval Postgraduate School
   Monterey, California